ARTICLE

doi:10.1038/nature11964

SCF^{FBXL3} ubiquitin ligase targets cryptochromes at their cofactor pocket

Weiman Xing[1,2], Luca Busino[3], Thomas R. Hinds[1], Samuel T. Marionni[4], Nabiha H. Saifee[1], Matthew F. Bush[4], Michele Pagano[3,5] & Ning Zheng[1,2]

The cryptochrome (CRY) flavoproteins act as blue-light receptors in plants and insects, but perform light-independent functions at the core of the mammalian circadian clock. To drive clock oscillations, mammalian CRYs associate with the Period proteins (PERs) and together inhibit the transcription of their own genes. The SCF^{FBXL3} ubiquitin ligase complex controls this negative feedback loop by promoting CRY ubiquitination and degradation. However, the molecular mechanisms of their interactions and the functional role of flavin adenine dinucleotide (FAD) binding in CRYs remain poorly understood. Here we report crystal structures of mammalian CRY2 in its apo, FAD-bound and FBXL3–SKP1-complexed forms. Distinct from other cryptochromes of known structures, mammalian CRY2 binds FAD dynamically with an open cofactor pocket. Notably, the F-box protein FBXL3 captures CRY2 by simultaneously occupying its FAD-binding pocket with a conserved carboxy-terminal tail and burying its PER-binding interface. This novel F-box-protein–substrate bipartite interaction is susceptible to disruption by both FAD and PERs, suggesting a new avenue for pharmacological targeting of the complex and a multifaceted regulatory mechanism of CRY ubiquitination.

Cryptochromes (CRYs) are evolutionarily conserved FAD-binding proteins that share close sequence homology with DNA photolyases and are widespread in both plant and animal kingdoms[1,2]. Using FAD as a chromophore, plant cryptochromes function as blue-light photoreceptors and regulate a broad range of light responses during plant growth and development[1,3]. In animals, cryptochromes are classified into two types[4,5]. Type I cryptochromes, exemplified by *Drosophila melanogaster* CRY, maintain blue-light sensitivity and have a key role in photic entrainment of the insect circadian clock[6], whereas type II cryptochromes are photo-insensitive and evolved as central components of the molecular clock[7,8].

Mammalian CRYs, the prototypic type II cryptochromes, act together with PERs, CLOCK and BMAL1 (brain and muscle aryl hydrocarbon receptor nuclear translocator-like protein 1) to constitute a transcription negative feedback loop that oscillates with a circadian periodicity of approximately 24 h (ref. 9). In this molecular clockwork, CLOCK and BMAL1 heterodimerize and activate the transcription of *CRY* and *PER* genes, whose protein products in turn form complexes in the cytoplasm and translocate into the nucleus to suppress their own gene expression by binding and inhibiting CLOCK–BMAL1 (refs 10, 11). In mammals, this basic clock circuitry drives the circadian oscillations of both the master clock in the brain and the peripheral clocks throughout the body[9,12]. The master clock is synchronized to light–dark cycles perceived by the retina and coordinates clocks in the peripheral tissues through a variety of mechanisms, such as feeding behaviour, body temperature and hormonal secretion[13–15].

Despite their functional divergence, many plant and animal cryptochromes are functionally linked to protein ubiquitination and degradation. For example, light-activated *Arabidopsis thaliana* CRY1 mediates seedling photomorphogenesis by inhibiting COP1 ubiquitin ligase[16,17], whereas *Drosophila* CRY modulates the insect circadian rhythm by promoting light-dependent degradation of the clock protein Timeless (TIM) and itself via the Jetlag ubiquitin ligase[18,19]. In both cases, photo-excitation of FAD is thought to induce conformational changes within the cryptochrome proteins and alter their interactions with the target proteins[20,21]. Recent biochemical and genetic studies have shown that mammalian CRYs are also functionally connected to the ubiquitin–proteasome system[22–24]. The SCF^{FBXL3} ubiquitin ligase complex (SKP1–CUL1–F-box protein complex containing the F-box protein FBXL3) has been identified to regulate the clock by promoting the degradation of CRYs.

As an integral part of the clock circuitry, SCF^{FBXL3}-catalysed CRY degradation needs to be regulated tightly. Indeed, the AMP-activated protein kinase (AMPK), a cellular metabolic sensor, has been shown to phosphorylate mouse CRY1 and accelerate its degradation by enhancing CRY1 binding to FBXL3 (ref. 25). Moreover, a recent circadian chemical screen has identified a period-lengthening small molecule that can compete with FAD for CRY binding and stabilize CRYs by inhibiting their ubiquitination[26]. These activities of the compound suggest that SCF^{FBXL3}-mediated CRY ubiquitination may be tuneable by the FAD cofactor, whose function in mammalian CRYs remains elusive[2]. To provide the missing structural framework for understanding the functions of mammalian CRYs and the regulatory mechanisms of CRY–FBXL3 interaction, we report here the crystal structures of mammalian CRY2 in three different functional forms.

Structure of murine apo CRY2 PHR

Cryptochromes in general contain a conserved photolyase-homology region (PHR) and a unique cryptochrome C-terminal (CCT) extension (CCE) (Supplementary Fig. 1a). We first determined the 2.7 Å crystal structure of the proteolytically stable mouse CRY2 PHR domain (amino acids 1–512) (Supplementary Fig. 2 and Supplementary Table 1). As expected, murine CRY PHR adopts a canonical photolyase

[1]Department of Pharmacology, Box 357280, University of Washington, Seattle, Washington 98195, USA. [2]Howard Hughes Medical Institute, University of Washington, Seattle, Washington 98195, USA. [3]Department of Pathology, NYU Cancer Institute, New York University School of Medicine, 522 First Avenue, SRB 1107, New York, New York 10016, USA. [4]Department of Chemistry, Box 351700, University of Washington, Seattle, Washington 98195, USA. [5]Howard Hughes Medical Institute, New York University School of Medicine, 522 First Avenue, SRB 1107, New York, New York 10016, USA.

fold, consisting of an amino-terminal α/β domain (N-terminal domain containing both α-helices and β-sheets), a C-terminal α-helical domain, and a connecting linker sequence (Fig. 1a). At the sequence level, vertebrate CRYs are more homologous to metazoan (6-4) photolyases than plant or type I animal cryptochromes (Supplementary Table 2). After superposition, murine CRY2 PHR can be aligned with the most homologous structure of *Drosophila* (6-4) photolyase with a root mean squared deviation (r.m.s.d.) of 1.1 Å over 431 equivalent Cα positions (Supplementary Fig. 3). However, unlike all known structures of (6-4) photolyases and cryptochromes[27], the murine CRY2 PHR structure represents the apo form of the flavoprotein (Fig. 1a). We found no electron density of FAD at its expected cofactor-binding pocket, despite the well-defined and conserved FAD-binding cavity[28]. This feature is in agreement with previous reports showing that only a small fraction of mammalian CRYs contains FAD when isolated from mammalian cells or various heterologous systems[2]. Similar to *Drosophila* (6-4) photolyase, murine CRY2 PHR does not co-purify with a second cofactor that acts as a light-harvesting antenna in some bacterial photolyases[20,28–31].

Structure of FAD-bound murine CRY2 PHR

Oxidized FAD is naturally fluorescent with an emission maximum at approximately 525 nm. In the presence of excess murine CRY2 PHR, FAD fluorescence is strongly quenched, suggesting that murine CRY2 PHR still retains specific FAD-binding activity (Fig. 1b). By titrating the amount of protein added, we estimated that FAD binds to isolated CRY2 PHR with an apparent dissociation constant (K_d) of approximately 40 μM (Fig. 1b). We next crystallized murine CRY2 PHR together with FAD and obtained a 2.2 Å resolution structure of the holoenzyme (Supplementary Table 1). As anticipated, FAD docks into the predicted cofactor pocket of murine CRY2 PHR and adopts the characteristic U-shaped conformation as seen in other cryptochrome and photolyase structures (Fig. 1c). Superposition analysis shows that its binding mode is nearly identical to that revealed in the *Drosophila* (6-4) photolyase structure (Fig. 1d).

A closer structural comparison, nevertheless, reveals a marked difference at the cofactor-binding site between murine CRY2 PHR and

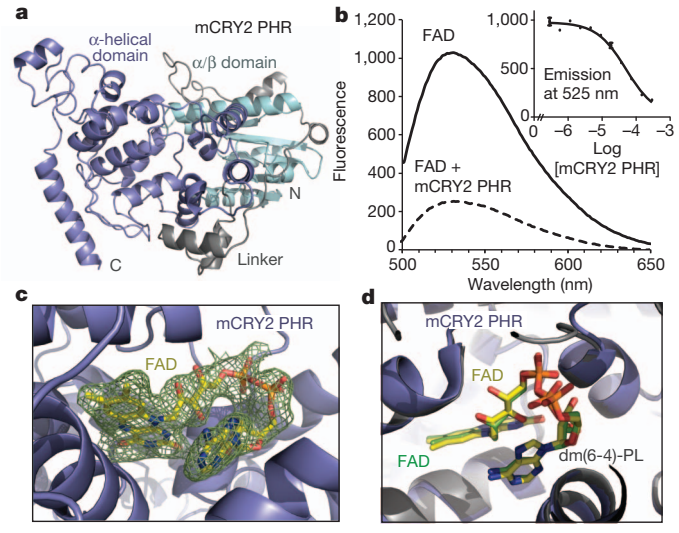

Figure 1 | Structure of murine CRY2 PHR in apo- and FAD-bound forms. **a**, Overall structure of the apo-bound form of the mouse CRY2 PHR (mCRY2 PHR) domain. **b**, mCRY2 PHR induced quenching of FAD fluorescence. The inset shows FAD-fluorescence quenching with mCRY2 PHR concentration titrated. Error bars, s.d. **c**, A close-up view of FAD bound to mCRY2 PHR with positive $F_o - F_c$ electron density contoured at 1.5 σ and calculated before the cofactor was built (green mesh). **d**, mCRY2 PHR and the *Drosophila* (6-4) photolyase (dm(6-4)-PL) are superimposed, with their FAD cofactors shown as sticks and their FAD carbon atoms in yellow and green, respectively.

other family members. In plant and insect (6-4) photolyases and cryptochromes, FAD is largely sequestered and buried deep inside the pocket as a prosthetic group[20,28–30]. In marked contrast, the cofactor is only partially embedded in murine CRY2 PHR, with one side of its adenosine diphosphate group fully exposed to the solvent (Fig. 2a, b). This unusual exposure of the cofactor can be attributed to the unique features of two adjacent structural elements in murine CRY2 PHR, the phosphate loop (a surface loop previously named for its phosphate-binding activity) and the protrusion motif. In *Drosophila* and *Arabidopsis* (6-4) photolyases, the adenosine moiety of FAD is mostly hidden under the well-ordered phosphate loop[28,30]. This loop harbours a central lysine residue that hydrogen bonds with the FAD adenine N7 atom and is secured further by a nearby sequence known as the protrusion motif (Fig. 2c). In murine CRY2 PHR, the protrusion motif is shifted far away from FAD, whereas the phosphate loop becomes completely disordered in the crystal (Fig. 2c). These local structural variations in CRY2 result in an overall open conformation of the FAD-binding pocket, which might explain the moderate affinity of FAD.

Overall structure of FBXL3–SKP1–CRY2

The unique CCEs of vertebrate CRYs share a strictly conserved 11-amino-acid segment (conserved CCE sequence, CCS), which is followed by a highly variable C-terminal region (Supplementary Fig. 1b). Using a protein co-expression strategy, we noticed that the nearly full-length form of murine CRY2 (amino acids 1–544) with the intact CCS motif can form a stable complex with FBXL3–SKP1. This prompted us to crystallize and determine a 2.8 Å resolution structure of the heterotrimeric complex (Supplementary Table 1).

The overall architecture of the CRY2–FBXL3–SKP1 complex resembles an ice-cream cone with the globular CRY2 sitting on top of the cup-shaped FBXL3–SKP1 complex (Fig. 3). The FBXL3 protein harbours a canonical 3-helix F-box motif that interacts with the SCF adaptor protein SKP1, and its C-terminal leucine-rich-repeat (LRR) domain folds into a curved and sickle-shaped solenoid structure, whose concave surface wraps around the α-helical domain and the CCS region of CRY2 opposite to the α/β domain (Fig. 3 and Supplementary Fig. 4). The FBXL3–CRY2 complex buries more than 4,800 $Å^2$ solvent accessible surface area and spontaneously assembles in a phosphorylation-independent manner, which was confirmed by native protein mass spectrometry (Supplementary Fig. 5).

The FBXL3 LRR domain

The FBXL3 LRR domain contains 12 LRRs that pack in tandem to produce a semicircular arch (Fig. 4a). The solenoid topology of the LRRs dictates that the concave surface of the arch is formed by the parallel β-strands of the repeats and the convex side is decorated by the α-helices. We refer to the topside of the arch that is lined with intra-repeat loops as the apical ridge (Fig. 4b).

Although the FBXL3 LRRs fold into a continuous single domain, it can be separated into two obvious halves as suggested by a prominent structural irregularity in LRR7 and LRR8. Compared to the six N-terminal LRRs, LRR7 has a much longer β-strand, which causes a significant offset at the apical ridge (Fig. 4b). This feature continues in LRR8, but is lost in LRR9 to LRR12. With a similar offset at the basal side between LRR8 and LRR9, all four C-terminal LRRs seem to be shifted up, relative to the six N-terminal repeats. Overall, LRR7 and LRR8 mediate this spatial displacement and this hints at a possible gene fusion event when *FBXL3* evolved in vertebrates. We name the two halves of FBXL3 LRRs as LRR-N (LRR1–LRR6) and LRR-C (LRR7–LRR12).

A quick inspection of the FBXL3 LRR–CRY2 interface reveals that the two halves of the FBXL LRR domain have unequal roles in engaging the cryptochrome protein. All six repeats in LRR-C are in close contact with the α-helical domain of CRY2, whereas most parts of LRR-N, except its four apical loops, are separated from CRY2 by a gap (Fig. 4c). Consistent with a more important role of LRR-C in recruiting CRY2,

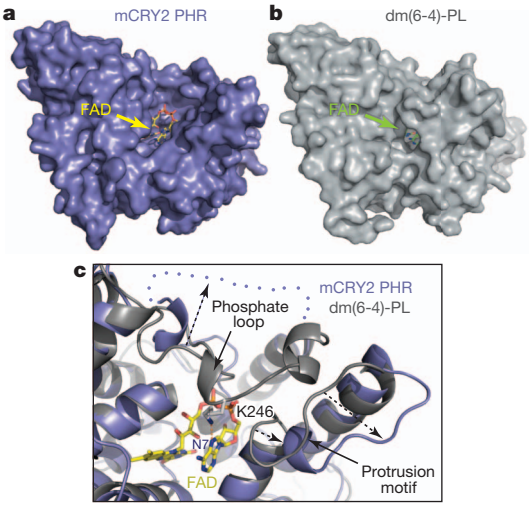

Figure 2 | The open FAD-binding pocket of murine CRY2 PHR. **a, b**, Surface representations of mCRY2 PHR and *Drosophila* (6-4) photolyase with their associated FAD cofactors shown as sticks. **c**, A close-up view of the open FAD-binding pocket of mCRY2–PHR shown with FAD as sticks and *Drosophila* (6-4)-photolyase superimposed (ribbons). Dotted blue line, disordered mCRY2 phosphate loop; dashed arrows, the differences of the phosphate loop and protrusion motif in the two proteins, respectively.

the missense mutations in the alleles known as after hours and overtime, Cys358Ser and Ile364Thr substitutions, are mapped to LRR10 and LRR11, respectively (Fig. 4c and Supplementary Fig. 6). Because both residues are located in the hydrophobic core of the LRR fold, their substitution by polar amino acids probably perturbs the local conformation of LRR-C.

The C-terminal tail of FBXL3

The C-terminal tail of FBXL3 represents the hallmark of the FBXL3–CRY2 interface by sticking out from the flat concave surface of LRR-C and penetrating into CRY2 (Fig. 5a). The 12-amino-acid C-terminal region of FBXL3 is mostly invariant in vertebrates and terminates with a tryptophan residue (Supplementary Fig. 6). This sequence caps the LRR solenoid and then takes a sharp turn at Pro 422, inserting the 5 amino acids closest to the C terminus into the α-helical domain of CRY2 (Supplementary Fig. 7). Notably, the last residue of the tail, Trp 428, reaches the core of the FAD-binding pocket and physically occupies the cofactor site.

Superposition analysis shows that the FBXL3 C-terminal tail approaches the FAD-binding pocket from the same angle as the (6-4) DNA lesion approaches the FAD-binding pocket in the *Drosophila*

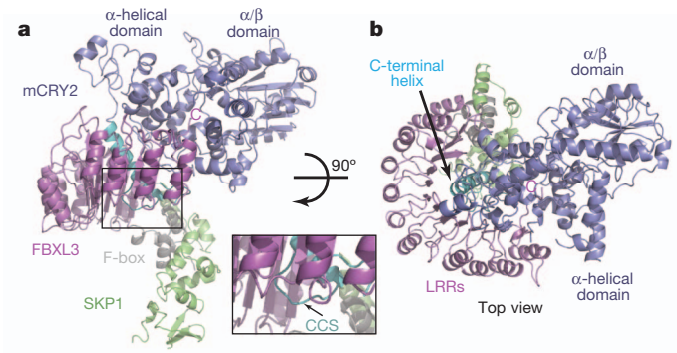

Figure 3 | Overall structure of the CRY2–FBXL3–SKP1 complex. **a**, Ribbon diagrams of the complex containing mCRY2 (blue), FBXL3 (magenta) and SKP1 (green). C, carboxyl terminus of FBXL3. The C-terminal helix and the CCS region in mCRY2 are shown in cyan and the F-box domain of FBXL3 is in grey. The inset shows a close-up view of the mCRY2 CCS region. **b**, Orthogonal view of the CRY2–FBXL3–SKP1 complex as shown in **a**.

(6-4) photolyase-DNA complex structure[30] (Fig. 5b). To expand the entrance, Met 425 of FBXL3 pushes aside an important CRY2 loop, which we name the interface loop. To enter the pocket, the FBXL3 tail stacks its Pro 426 residue against Trp 310 of CRY2 and flips the side chain of CRY2 His 373 with Thr 427 (Fig. 5c, d). In the FAD-bound form, these CRY2 residues directly contact the cofactor. Inside the pocket, the side chain of FBXL3 Trp 428 occupies the central space of the cavity, which corresponds to the narrow gap between the isoalloxazine and adenine rings of FAD. While donating a hydrogen bond to the backbone carbonyl group of Gln 307 in CRY2, the indole ring of Trp 428 makes multiple hydrophobic contacts with CRY2. The carboxyl group of Trp 428 forms additional hydrogen bonds with CRY2 Ser 414 and a signature arginine residue, Arg 376 (Fig. 5c, d). Overall, this network of interactions anchors the FBXL3 tail at the very centre of the FAD-binding pocket, predicting that FAD and the F-box protein will compete to bind the cryptochrome protein.

Interface between FBXL3 and CRY2 PHR

In addition to the C-terminal tail, the FBXL3 LRR domain also forms extensive interfaces with CRY2 through its solenoid fold. At the apical ridge of LRR-N, four FBXL3 loops from LRR1–LRR4 interact with the back of the α-helical domain of CRY2 opposite to the FAD-binding pocket (Figs 3b and 4c). This part of the interface is mediated largely by polar interactions (Supplementary Fig. 7).

In contrast to LRR-N, the FBXL3 LRR-C subdomain binds CRY2 through a predominantly hydrophobic interface. On its concave wall, LRR-C presents a cluster of more than ten hydrophobic residues strictly

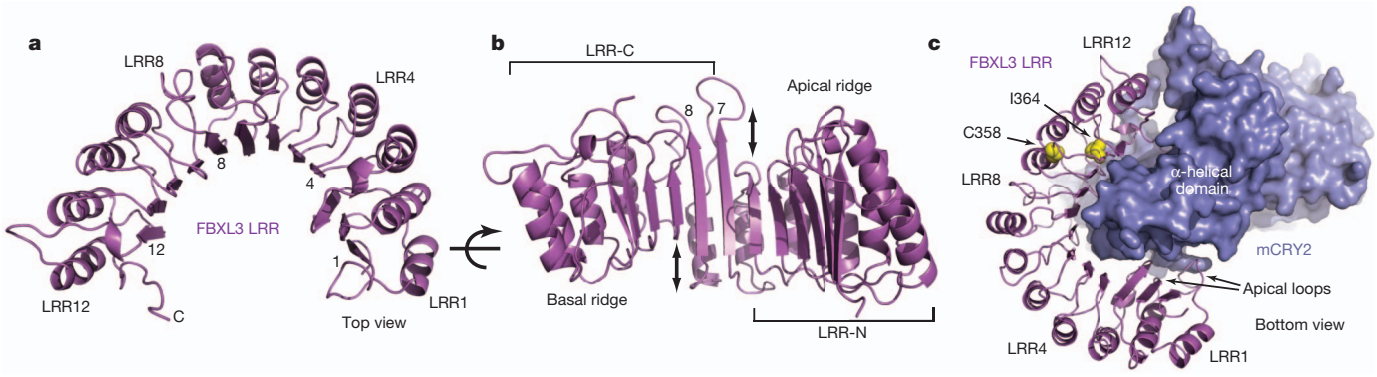

Figure 4 | Structure of the FBXL3 LRR domain. **a**, Ribbon diagrams of the LRR domain of FBXL3 with its complete C-terminal tail. Select LRRs are labelled and numbered at their helices and β-strands. **b**, An orthogonal view of the LRR domain shown in **a**. Double-ended arrows indicate the offset between LRR6 and LRR7, and between LRR8 and LRR9. **c**, A bottom view of the FBXL3 LRR domain (magenta) bound to mCRY2 (blue). Side chains of the FBXL3 residues mutated in the overtime and after hours alleles are shown as yellow spheres.

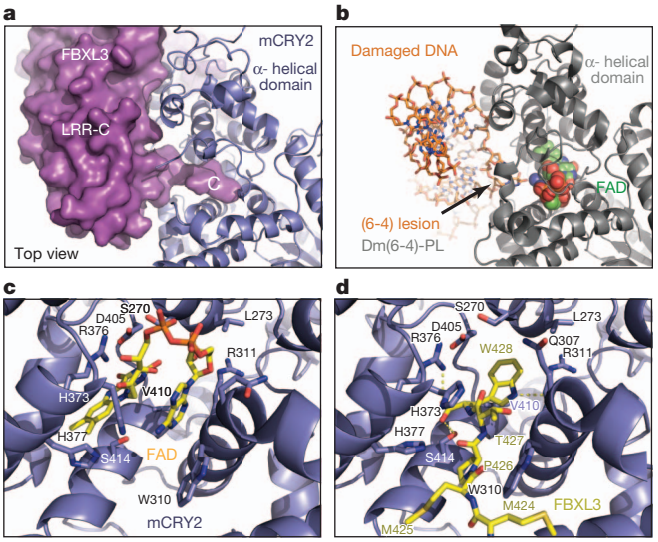

Figure 5 | Interaction between the FBXL3 C-terminal tail and the CRY2 FAD-binding pocket. **a**, Surface representation of the FBXL3 LRR-C subdomain with its C-terminal tail inserted into the FAD-binding pocket of mCRY2 (blue ribbons). **b**, The structure of *Drosophila* (6-4) photolyase–DNA complex shown from the same orientation as mCRY2 in **a**. FAD is shown as spheres. The damaged DNA substrate is shown as a stick diagram. **c, d**, A close-up view of the mCRY2 FAD-binding pocket showing key FAD- and FBXL3-interacting residues. FAD and the FBXL3 tail are shown as sticks. Dashed yellow lines represent hydrogen bonds.

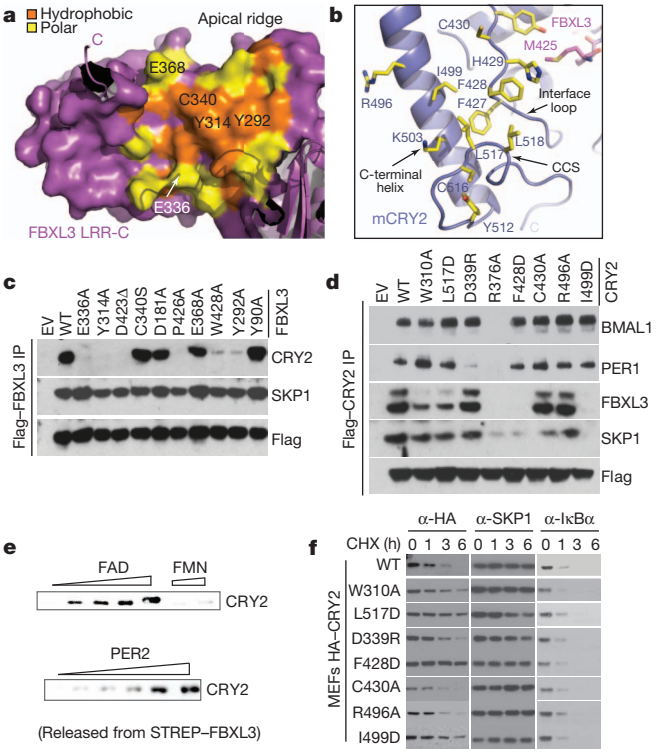

Figure 6 | Structural and functional analyses of the FBXL3–murine CRY2 interface. **a**, Surface and ribbon diagrams of the FBXL3 LRR-C subdomain showing hydrophobic and polar residues that are involved in mCRY2 binding. Amino acids selected for mutational analyses are labelled. The C-terminal tail and some N-terminal repeats are shown as ribbon diagrams. **b**, Ribbon diagrams of the mCRY2 structural elements involved in FBXL3 LRR-C interaction. Select interface residues are shown as sticks. A part of the FBXL3 tail (magenta) is shown for reference. **c**, Interactions of retrovirus-expressed FBXL3 mutants with endogenous mCRY2 in mouse embryonic fibroblasts (MEF) assessed by co-immunoprecipitation (IP) and western blot analysis. **d**, Flag–mCRY2 complexes were immunoprecipitated with an anti-Flag resin from transfected HEK293T cells and assessed for binding to FBXL3, PER1, BMAL1 and SKP1. Arg376Ala served as a negative control as it is probably detrimental to mCRY2 folding (see Supplementary Discussion for Cys430Ala and FBXL3–Cys340Ser mutants). **e**, Two *in vitro* competition assays showing the ability of FAD and PER2, but not FMN, to disrupt a preformed FBXL3–mCRY2 complex. **f**, MEFs were infected with retroviruses expressing either mCRY2 or mCRY2 mutants and treated with cycloheximide (CHX) for the indicated time in hours. Total extracts were examined by immunoblot analysis.

conserved in vertebrate CRYs (Fig. 6a and Supplementary Fig. 6). These residues, plus a circle of peripheral polar amino acids, recognize a large complementary surface on CRY2 adjacent to the cofactor pocket. The interface on the CRY2 side is constructed by three key structural motifs; the interface loop, the C-terminal helix and the CCS region (Fig. 6b). With a string of strictly conserved aromatic residues (Supplementary Fig. 8), the CRY2 interface loop is buttressed by Met 425 from the FBXL3 tail on one side and the CRY2 C-terminal helix on the other. The CRY2 CCS region adopts a well-ordered loop structure that wraps back onto the interface loop and the C-terminal helix. Together, these three motifs contribute a panel of hydrophobic residues grouped at the centre of the LRR-C binding interface. By making direct contacts with both FBXL3 and CRY2 PHR, the conserved CCS region of CRY2 probably takes up its structural role at the interface through an 'induced fit' mechanism (Supplementary Fig. 9).

To map regions that are critical for FBXL3–CRY2 interaction, we tested the binding activity of a series of FBXL3 and CRY2 mutants. Disruption of interactions at the apical ridge of LRR-N did not affect the complex formation (Asp181Ala and Tyr90Ala (Fig. 6c), Asp339Arg and Arg496Ala (Fig. 6d and Supplementary Fig. 7)), indicating a supportive role of LRR-N in recruiting CRY2. By contrast, CRY2 binding was impaired severely by either single amino acid substitution or truncation of the FBXL3 tail (Pro426Ala, Trp428Ala, Asp423Δ (Fig. 6c)). Similarly, alteration of a CRY2 residue in the cofactor pocket also compromised complex association (Trp310Ala (Fig. 5d, 6d)). These results pinpoint the FBXL3 C-terminal tail as a 'hot spot' of the interface and suggest a possible antagonistic role of FAD in regulating the FBXL3–CRY2 interaction. In a purified system, we confirmed that free FAD, but not flavin mononucleotide (FMN), was sufficient to disrupt a pre-formed FBXL3–CRY2 complex in a dose-dependent manner (Fig. 6e).

Our mutagenesis analysis also established the FBXL3 LRR-C subdomain as a second critical docking site for CRY2. Mutations of individual aromatic residues at the hydrophobic concave wall of LRR-C or a nearby CCS-interacting residue effectively abolished CRY2 binding (Tyr292Ala, Tyr314Ala and Glu336Ala (Fig. 6a, c and Supplementary Fig. 9)). The same effect was seen when a single hydrophobic-to-charged mutation was introduced to each of the three LRR-C-interacting structural motifs in CRY2; that is, the interface loop (Phe428Asp), the C-terminal helix (Ile499Asp) and the CCS region (Leu517Asp) (Fig. 6b, d). The functional importance of this part of the interface and the FBXL3 tail-gripping pocket was underscored further by the stabilization of the CRY2 mutants with hot-spot residues altered at these sites (Fig. 6f and Supplementary Fig. 9).

The C-terminal helix of CRY2 and its two basic residues, Arg 501 and Lys 503, are thought to be essential for PER binding[32,33]. In complex with FBXL3, the entire CRY2 C-terminal helix is masked by the LRR domain of the F-box protein (Fig. 3b and Supplementary Fig. 9). We found by chance that mutation of Asp 339, which is in close proximity to Arg 501, also showed defective interaction with PER1 (Fig. 6d and Supplementary Fig. 7). These lines of evidence strongly suggest that PERs and FBXL3 share an overlapping CRY2-binding interface, which should prevent them from binding CRY2 simultaneously. Indeed, PER2-bound CRY2 is completely devoid of FBXL3 (Supplementary Fig. 10). Importantly, just like FAD, a purified C-terminal fragment of PER2, which corresponds to a previously mapped minimal CRY-binding region[34], was able to dislodge CRY2 from FBXL3 (Fig. 6e). We were able

to confirm that the abundance of PER2 had a direct effect on the stability of both CRY1 and CRY2 (Supplementary Fig. 10)[34,35], probably by competing with the SCF^{FBXL3} E3 ligase.

Discussion

The structure of the mammalian cryptochrome reveals an unexpected open FAD-binding pocket that probably evolved in vertebrates to enable dynamic FAD binding. This unique property is built on the plasticity of the phosphate loop guarding the entrance of the pocket. Intriguingly, this loop is highly conserved among vertebrates (Supplementary Fig. 8), raising the possibility that its alteration by phosphorylation[25,36] or CRY-binding proteins might regulate the affinity of FAD (Supplementary Fig. 11).

Importantly, our structural results have unravelled the functional requirement for the dynamic FAD-binding pocket in CRYs and a novel mechanism of substrate-recognition by the SCF ubiquitin ligase. In contrast to the canonical degron-based substrate-engagement scheme[37,38], FBXL3 takes advantage of the deep but accessible cofactor pocket of CRYs to capture the substrate (Supplementary Fig. 12). This interaction mode establishes FAD and its analogues as potential pharmacological agents for controlling clock oscillation by competing with SCF^{FBXL3}. Such an effect might be achieved by the CRY-stabilizing compounds identified in the recent circadian chemical screen[26].

The unexpected interface between CRY2 and FBXL3 suggests that their interactions can be regulated by multiple mechanisms. As a common metabolic redox cofactor in the cell, it is possible that FAD directly controls the stability of CRYs by competing with the ubiquitin ligase. Although oxidized FAD binds murine CRY2 with a modest affinity (see Supplementary Discussion), its interaction with the CRY proteins can be influenced by its redox states and several factors mentioned above. The CRY2–FBXL3 structure also supports the idea that PERs may have a role in stabilizing CRYs by shielding them from SCF^{FBXL3}. This function is reminiscent of the stabilization of PERs by CRYs against $SCF^{\beta TrCP}$-mediated degradation[11,34]. Such interplay between the two obligate functional partners could serve as a mechanism for synchronizing their stability to ensure robust clock oscillation and phase shift. In fact, the CRY1-destabilizing effect of Ser 71 phosphorylation by AMPK may be partially explained by its reported activity in blocking PER2 binding[25].

METHODS SUMMARY

The full Methods provides detailed information about all experimental procedures, including description of protein purification; protein crystallization, data collection and structure determination; FAD fluorescence assay; *in vitro* competition assay; and mutagenesis, cell culture, binding and stability analyses.

Full Methods and any associated references are available in the online version of the paper.

Received 21 August 2012; accepted 29 January 2013.
Published online 17 March 2013.

1. Chaves, I. *et al.* The cryptochromes: blue light photoreceptors in plants and animals. *Annu. Rev. Plant Biol.* **62,** 335–364 (2011).
2. Oztürk, N. *et al.* Structure and function of animal cryptochromes. *Cold Spring Harb. Symp. Quant. Biol.* **72,** 119–131 (2007).
3. Lin, C. & Shalitin, D. Cryptochrome structure and signal transduction. *Annu. Rev. Plant Biol.* **54,** 469–496 (2003).
4. Yuan, Q., Metterville, D., Briscoe, A. D. & Reppert, S. M. Insect cryptochromes: gene duplication and loss define diverse ways to construct insect circadian clocks. *Mol. Biol. Evol.* **24,** 948–955 (2007).
5. Zhu, H. *et al.* The two CRYs of the butterfly. *Curr. Biol.* **15,** R953–R954 (2005); erratum **16,** 730 (2006).
6. Stanewsky, R. *et al.* The cry^b mutation identifies cryptochrome as a circadian photoreceptor in *Drosophila*. *Cell* **95,** 681–692 (1998).
7. van der Horst, G. T. *et al.* Mammalian Cry1 and Cry2 are essential for maintenance of circadian rhythms. *Nature* **398,** 627–630 (1999).
8. Griffin, E. A., Staknis, D. & Weitz, C. J. Light-independent role of CRY1 and CRY2 in the mammalian circadian clock. *Science* **286,** 768–771 (1999).
9. Reppert, S. M. & Weaver, D. R. Coordination of circadian timing in mammals. *Nature* **418,** 935–941 (2002).
10. Shearman, L. P. *et al.* Interacting molecular loops in the mammalian circadian clock. *Science* **288,** 1013–1019 (2000).
11. Lee, C., Etchegaray, J. P., Cagampang, F. R., Loudon, A. S. & Reppert, S. M. Posttranslational mechanisms regulate the mammalian circadian clock. *Cell* **107,** 855–867 (2001).
12. Dibner, C., Schibler, U. & Albrecht, U. The mammalian circadian timing system: organization and coordination of central and peripheral clocks. *Annu. Rev. Physiol.* **72,** 517–549 (2010).
13. Green, C. B., Takahashi, J. S. & Bass, J. The meter of metabolism. *Cell* **134,** 728–742 (2008).
14. Bass, J. & Takahashi, J. S. Circadian integration of metabolism and energetics. *Science* **330,** 1349–1354 (2010).
15. Asher, G. & Schibler, U. Crosstalk between components of circadian and metabolic cycles in mammals. *Cell Metab.* **13,** 125–137 (2011).
16. Yang, H. Q., Tang, R. H. & Cashmore, A. R. The signaling mechanism of *Arabidopsis* CRY1 involves direct interaction with COP1. *Plant Cell* **13,** 2573–2587 (2001).
17. Wang, H., Ma, L. G., Li, J. M., Zhao, H. Y. & Deng, X. W. Direct interaction of *Arabidopsis* cryptochromes with COP1 in light control development. *Science* **294,** 154–158 (2001).
18. Peschel, N., Chen, K. F., Szabo, G. & Stanewsky, R. Light-dependent interactions between the *Drosophila* circadian clock factors Cryptochrome, Jetlag, and Timeless. *Curr. Biol.* **19,** 241–247 (2009).
19. Koh, K., Zheng, X. & Sehgal, A. JETLAG resets the *Drosophila* circadian clock by promoting light-induced degradation of TIMELESS. *Science* **312,** 1809–1812 (2006).
20. Zoltowski, B. D. *et al.* Structure of full-length *Drosophila* cryptochrome. *Nature* **480,** 396–399 (2011).
21. Liu, B., Liu, H., Zhong, D. & Lin, C. Searching for a photocycle of the cryptochrome photoreceptors. *Curr. Opin. Plant Biol.* **13,** 578–586 (2010).
22. Busino, L. *et al.* SCF^{FBXL3} controls the oscillation of the circadian clock by directing the degradation of cryptochrome proteins. *Science* **316,** 900–904 (2007).
23. Godinho, S. I. *et al.* The after-hours mutant reveals a role for Fbxl3 in determining mammalian circadian period. *Science* **316,** 897–900 (2007).
24. Siepka, S. M. *et al.* Circadian mutant *Overtime* reveals F-box protein FBXL3 regulation of *Cryptochrome* and *Period* gene expression. *Cell* **129,** 1011–1023 (2007).
25. Lamia, K. A. *et al.* AMPK regulates the circadian clock by cryptochrome phosphorylation and degradation. *Science* **326,** 437–440 (2009).
26. Hirota, T. *et al.* Identification of small molecule activators of cryptochrome. *Science* **337,** 1094–1097 (2012).
27. Müller, M. & Carell, T. Structural biology of DNA photolyases and cryptochromes. *Curr. Opin. Struct. Biol.* **19,** 277–285 (2009).
28. Hitomi, K. *et al.* Functional motifs in the (6–4) photolyase crystal structure make a comparative framework for DNA repair photolyases and clock cryptochromes. *Proc. Natl Acad. Sci. USA* **106,** 6962–6967 (2009).
29. Brautigam, C. A. *et al.* Structure of the photolyase-like domain of cryptochrome 1 from *Arabidopsis* thaliana. *Proc. Natl Acad. Sci. USA* **101,** 12142–12147 (2004).
30. Maul, M. J. *et al.* Crystal structure and mechanism of a DNA (6–4) photolyase. *Angew. Chem. Int. Edn Engl.* **47,** 10076–10080 (2008).
31. Park, H. W., Kim, S. T., Sancar, A. & Deisenhofer, J. Crystal structure of DNA photolyase from *Escherichia coli*. *Science* **268,** 1866–1872 (1995).
32. Ozber, N. *et al.* Identification of two amino acids in the C-terminal domain of mouse CRY2 essential for PER2 interaction. *BMC Mol. Biol.* **11,** 69 (2010).
33. Chaves, I. *et al.* Functional evolution of the photolyase/cryptochrome protein family: importance of the C terminus of mammalian CRY1 for circadian core oscillator performance. *Mol. Cell. Biol.* **26,** 1743–1753 (2006).
34. Yagita, K. *et al.* Nucleocytoplasmic shuttling and mCRY-dependent inhibition of ubiquitylation of the mPER2 clock protein. *EMBO J.* **21,** 1301–1314 (2002).
35. Chen, R. *et al.* Rhythmic PER abundance defines a critical nodal point for negative feedback within the circadian clock mechanism. *Mol. Cell* **36,** 417–430 (2009).
36. Sanada, K., Harada, Y., Sakai, M., Todo, T. & Fukada, Y. Serine phosphorylation of mCRY1 and mCRY2 by mitogen-activated protein kinase. *Genes Cells* **9,** 697–708 (2004).
37. Hao, B. *et al.* Structural basis of the Cks1-dependent recognition of $p27^{Kip1}$ by the SCF^{Skp2} ubiquitin ligase. *Mol. Cell* **20,** 9–19 (2005).
38. Tan, X. *et al.* Mechanism of auxin perception by the TIR1 ubiquitin ligase. *Nature* **446,** 640–645 (2007).

Supplementary Information is available in the online version of the paper.

Acknowledgements We thank the beamline staff of the Advanced Light Source at the University of California at Berkeley for help with data collection, and members of the Zheng laboratory for discussion. This work is supported by the Howard Hughes Medical Institute (N. Z. and M. P.), the National Institutes of Health (R01-CA107134 to N.Z., 5T32-HL007151 to L.B., and R01-GM057587, R37-CA-076584 and R21-CA161108 to M.P.), and the University of Washington (S.T.M. and M.F.B.).

Author Contributions The protein purification and crystallization experiments were conceived by W.X., L.B., M.P. and N.Z., initiated by N.H.S., and conducted by W.X. W.X. and N.Z. determined and analysed the structures. FAD fluorescence and *in vitro* competition experiments were conceived by W.X., T.R.H. and N.Z., and conducted by W.X. and T.R.H. Mutational and binding studies, and stability analyses were conceived by L.B., M.P., W.X. and N.Z., and conducted by L.B. S.T.M. and M.F.B. conducted native mass spectrometry experiments.

Author Information Structural coordinates and structural factors for FBXL3–CRY2–SKP1, CRY2–FAD and CRY2 are deposited in the Protein Data Bank under accession numbers 4I6J, 4I6G and 4I6E. Reprints and permissions information is available at www.nature.com/reprints. The authors declare no competing financial interests. Readers are welcome to comment on the online version of the paper. Correspondence and requests for materials should be addressed to N.Z. (nzheng@u.washington.edu).

METHODS

Recombinant protein purification. The mouse CRY2 (amino acids 1–544) was expressed as a glutathione S-transferase (GST) fusion protein in High Five (Invitrogen) suspension insect cells and isolated by glutathione affinity chromatography using buffer containing 50 mM Tris-HCl, pH 7.5, 300 mM NaCl, 10% Glycerol, 10 mM DTT (dithiothreitol) and 0.5 mM FAD. The protein was purified further by cation exchange and gel filtration chromatography after on-column cleavage by tobacco etch virus (TEV) protease. During purification, the polypeptide produced a series of C-terminal degradation products that were not affected by the presence or absence of FAD and dithionite. Two shorter versions of the protein, murine CRY2 with amino acids 1–527 and murine CRY2 with amino acids 1–512, were subsequently purified. Native mass spectrometry analysis confirmed that murine CRY2 with amino acids 1–512 was stable, but murine CRY2 with amino acids 1–527 was not (Supplementary Figs 1 and 2). The mouse CRY2 (amino acids 1–544) protein was co-expressed with full-length human FBXL3 and SKP1 in High Five suspension insect cells (human FXBL3 is 97% identical to mouse FBXL3, and the F-box and LRR regions of human and mouse FBXL3 differ by only 3 amino acids; Supplementary Fig. 6). FBXL3 was fused with an N-terminal GST tag, whereas the other two proteins were tag-free. The CRY2–FBXL3–SKP1 complex was isolated from the soluble cell lysate by glutathione affinity chromatography. After on-column tag cleavage by TEV, the complex was purified further by anion exchange and gel filtration chromatography and then concentrated by ultrafiltration to 10 mg ml^{-1} in a buffer of 20 mM Tris-HCl, pH 8.0, 200 mM NaCl, 5 mM DTT. Mouse PER2 (amino acids 1095–1235) was overexpressed as a GST-fusion protein in *Escherichia coli* and purified by glutathione affinity, anion exchange and gel filtration chromatography.

Crystallization, data collection and structure determination. The crystals of the CRY2–FBXL3–SKP1 complex were grown at 4 °C by the hanging-drop vapour diffusion method, using 1.5 µl protein complex sample mixed with an equal volume of reservoir solution containing 0.2 M ammonium citrate, 13–14% PEG3350 and 7% acetonitrile. Diffraction-quality crystals that were obtained were subjected to a post-crystallization dehydration procedure by gradually increasing the concentration of PEG3350 to 30%, and then directly frozen in liquid nitrogen. This procedure consistently improved the resolution of the crystals beyond approximately 4 Å. The CRY2–FBXL3–SKP1 derivative crystals were prepared by soaking the native crystals in the buffer containing 15% PEG3350 and 7% acetonitrile supplemented with 0.2 mM $KAu(CN)_2$ for 12 h, followed by soaking in 0.5 mM $KAu(CN)_2$ for 12 h and then 1 mM $KAu(CN)_2$ for a further 12 h. After soaking, the crystals were dehydrated by the same method as native crystals. The crystals of murine CRY2 were also grown at 4 °C by the hanging-drop vapour diffusion method with 1.5 µl protein mixed with an equal volume of reservoir solution containing 0.1 M MES- imidazole, pH 6.5, 7.2% PEG8K, 20% ethylene glycol (v/v), 0.03 M NaF, NaBr and NaI. The crystals were directly frozen in liquid nitrogen. The CRY2–FAD crystals were obtained by soaking the murine CRY2 crystals with 1 mM FAD in the reservoir buffer with extra 7.5% Glycerol for 2 h before freezing in liquid nitrogen. All data sets were collected at the BL8.2.1 and BL8.2.2 beamlines at the Advanced Light Source of the Lawrence Berkeley National Laboratory. Reflection data were indexed, integrated and scaled with the HKL2000 package[39]. The murine CRY2 PHR domain structure was determined by molecular replacement using the *Drosophila* (6-4) photolyase structure (PDB:3CVU) as the search model. Soaking with FAD altered the unit cell and substantially improved the murine CRY2 PHR domain crystals. For the apo structure, translation libration screw-motion (TLS) refinement was necessary to reduce the *R*-free value below 0.30. The CRY2–FBXL3–SKP1 structure was solved by molecular replacement combined with single-wavelength anomalous dispersion phases (MR-SAD) using the software PHENIX[40]. The structural models were manually built, refined and rebuilt with the programs COOT[41] and PHENIX[40].

FAD fluorescence assay. FAD fluorescence and binding studies were carried out in a PBS buffer, pH 7.4, with 10% glycerol at room temperature in a half-area 96-well plate with a total volume of 100 µl. Interaction was quantified by measuring the decrease in FAD fluorescence (excitation at 450 nm and emission at 520 nm) after binding to mouse CRY2. FAD concentration was held constant at 10 µM in all wells, and murine CRY2 PHR was serially diluted ten times from 300 µM to 292 nM. Nonspecific FAD binding (background) was measured in parallel with equal molar concentrations of ovalbumin or lysozyme, which do not bind FAD. All protein concentrations were run in duplicate. The binding data was fit using a standard nonlinear regression curve fitting method with a log(inhibitor) versus response model in Prism 5 (GraphPad Software).

***In vitro* competition assay.** Strep-tagged full-length FBXL3, GST-tagged murine CRY2 (amino acids 1–544) and His-tagged SKP1 were co-expressed in monolayer High Five insect cells. The complex was purified without elution by Strep-Tactin affinity resin in a buffer containing 100 mM Tris-HCl, pH 8.0, 300 mM NaCl and 20 mM DTT. The Strep-Tactin resin beads with the immobilized complex were subsequently aliquoted in a volume of 100 µl with 1 mg ml^{-1} total protein and placed in a panel of 7.5 mm gravity columns. The beads were incubated with 300 µl of oxidized FAD, FMN or purified murine PER2 (amino acids 1095–1235) in a serial dilution (FAD: 0, 5, 50, 500 µM and 5 mM; FMN: 50 and 500 µM; murine PER2: 0, 2.5, 5, 10, 20 and 40 µM) for 3 h at 4 °C. Flow-through and subsequent two-column-volume wash fractions were collected from each column and the GST–CRY2 protein released from the column was examined with SDS–PAGE and detected by western blot analysis using anti-GST antibody.

Cell culture. HEK293T cells were maintained in Dulbecco's modified Eagle's medium (DMEM) containing 10% bovine serum. Immortalized mouse embryonic fibroblasts (MEFs) were maintained in DMEM containing 10% fetal bovine serum (FBS). HEK293T cells were transfected with PEI (Polysciences) according to the manufacturer's instructions. Cyclohexemide (Sigma) was used at a final concentration of 100 µM. For retrovirus production, GP-293 packaging cells (Clontech) were used. Forty-eight hours after transfection, the virus-containing medium was collected and supplemented with 8 µg ml^{-1} polybrene (Sigma). Cells were then infected by replacing the cell culture medium with the viral supernatant for six hours. Forty-eight hours after infection, cells were selected with 1 µg ml^{-1} puromycin.

Co-immunoprecipitation binding studies. Cells were collected and subsequently lysed in lysis buffer (50 mM Tris-HCl, pH 7.5, 150 mM NaCl, 1 mM EDTA, 50 mM NaF, 0.5% NP40, plus protease and phosphatase inhibitors). Immunoprecipitation was carried out with anti-Flag agarose beads (Sigma). Immuno-complexes were washed five times with lysis buffer and eluted in Laemmli buffer containing 1% SDS. Cell extracts or Flag-immunocomplexes were analysed by SDS–PAGE and then by immunoblot analysis with the following antibodies: anti-Flag (Sigma), anti-CRY1 and CRY2 (Bethyl), anti-PER1 (Alpha Diagnostic), anti-PER2 (Bethyl), anti-BMAL1 (Bethyl), anti-Skp1 (Invitrogen) and anti-FBXL3 (ref. 22).

Plasmids. Wild-type and mutant mouse CRY2 complementary DNAs were subcloned into pcDNA3.1–Flag. Mouse PER2 was cloned into pMT-Myc. For retrovirus production, cDNAs encoding Flag or HA-tagged FBXL3 or CRY2 wild-type and mutants, were subcloned into the retroviral vector pBabePuro (Cell Biolabs). Point mutations were generated using the QuikChange Site-directed Mutagenesis kit (Stratagene).

39. Otwinowski, Z. & Minor, W. In *Methods in Enzymology* Vol. 276 (eds Carter, C. W. & Sweet, R. M.) 307–326 (Academic Press, 1997).
40. Adams, P. D. *et al.* PHENIX: building new software for automated crystallographic structure determination. *Acta Crystallogr. D* **58,** 1948–1954 (2002).
41. Collaborative Computational Project, number 4. The *CCP*4 Suite: programs for protein crystallography. *Acta Crystallogr. D* **50,** 760–763 (1994).